16

Optical Metrology of Diffuse Surfaces

K. Creath, J. Schmit, and J. C. Wyant

This chapter discusses moiré, fringe projection, structured illumination, holographic interferometry, digital holography, and speckle interferometry techniques for testing diffuse surfaces. Diffuse surfaces may be ground optical surfaces; or more often than not, they are other types of engineering surfaces or human figures. The main applications of these techniques are to determine surface form and shape or to measure displacement due to stress and object motion. When measuring surface form, these techniques provide a coarser and more flexible means of testing a wider variety of surfaces than do conventional interferometers. For displacement measurement due to applied stress, static as well as time-average and dynamic displacements can be determined quantitatively. These techniques are used a lot in machine vision applications, for process control, and for specialized measurement tasks on engineering components. Applications range from measuring the shape of an airplane window to determining whether components will stay on a circuit board, to studying vibration modes of turbine blades, to monitoring the alignment of segments in a large segmented telescope, to making replicas of historic sculptures, producing a well-fitting pair of jeans, and creating animated movies or video games with realistic motion of live figures. The newest techniques pushing the limits of this technology currently focus on rapid prototyping and real-time shape observation for multimedia and security.

16.1. MOIRÉ AND FRINGE PROJECTION TECHNIQUES

16.1.1. Introduction

The term moiré is not the name of a person; in fact, it is a French word referring to ''an irregular wavy finish usually produced on a fabric by pressing between engraved rollers'' (*Webster's*, 1981). In optics, it refers to a beat pattern produced between two

Optical Shop Testing, Third Edition Edited by Daniel Malacara

gratings of approximately equal spacing. It can be seen in everyday things, such as the overlapping of two window screens, the rescreening of a half-tone picture, or with a striped shirt seen on television. The use of moiré for reduced sensitivity testing was introduced by Lord Rayleigh in 1874. Lord Rayleigh looked at the moiré between two identical gratings to determine their quality even though each individual grating could not be resolved under a microscope.

Fringe projection entails projecting a fringe pattern or grating on an object and viewing it from a different direction. The first use of fringe projection for determining surface topography was presented by Rowe and Welford in 1967. It is a convenient technique for contouring objects which are too coarse to be measured with standard interferometry. Fringe projection is related to optical triangulation using a single point of light and light sectioning where a single line is projected onto an object and viewed in a different direction to determine the surface contour (Case et al., 1987). These techniques are usually used with diffuse objects; however, alternative methods have been developed to measure specular surfaces by looking at the fringe reflection (Ritter and Hahn, 1983; Hang et al., 2000).

Moiré and fringe projection interferometry complement conventional holographic interferometry, especially for testing optics to be used at long wavelengths. Although two-wavelength holography (TWH) can be used to contour surfaces at any longer-than-visible wavelength, visible interferometric environmental conditions are required. Moiré and fringe projection interferometry can contour surfaces at any wavelength longer than 10–100 μm with reduced environmental requirements and no intermediate photographic recording setup. Moiré is also a useful technique for aiding in the understanding of interferometry.

This chapter explains what moiré is and how it relates to interferometry. Contouring techniques utilizing fringe projection, projection and shadow moiré, and two-angle holography are all described and compared. All of these techniques provide the same result and can be described by a single theory. The relationship between these techniques and the holographic and conventional interferometry will be shown. Errors caused by divergent geometries are described, and applications of these techniques combined with phase-measurement techniques are presented. Further information on these techniques can be found in the following books and book chapters: Varner (1974), Vest (1979), Hariharan (1984), Gasvik (2002), Chiang (1983) Patorski and Kujawinska (1993), Post et al. (1997), Amridror (2000), and Walker (2004).

16.1.2. What is Moiré?

Moiré patterns are extremely useful to help understand basic interferometry and interferometric test results. Figure 16.1 shows the moiré pattern (or beat pattern) produced by two identical straight line gratings rotated by a small angle relative to each other. A dark fringe is produced where the dark lines are out of step one-half period, and a bright fringe is produced where the dark lines for one grating fall on top of the corresponding dark lines for the second grating. If the angle between the two gratings is increased, the separation between the bright and dark

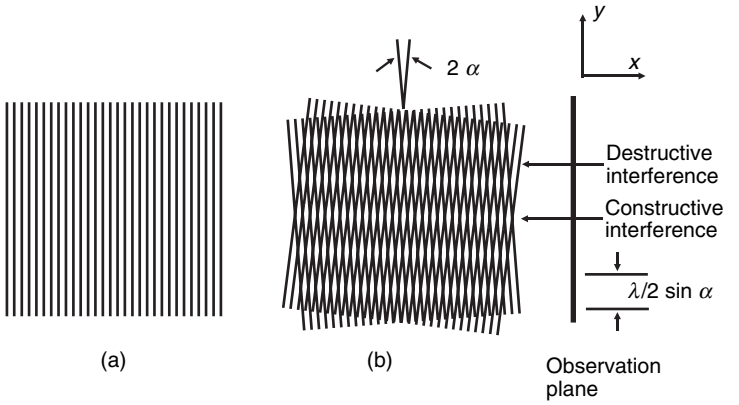

FIGURE 16.1. (a) Straight line grating. (b) Moiré between two straight line gratings of the same pitch at an angle 2α with respect to one another.

fringes decreases. (A simple explanation of moiré is given by Oster and Nishijima (1963).)

If the gratings are not identical to the straight line gratings, the moiré pattern (bright and dark fringes) will not be straight equi-spaced fringes. The following analysis shows how to calculate the moiré pattern for arbitrary gratings. Let the intensity transmission function for two gratings $f_1(x, y)$ and $f_2(x, y)$ be given by

$$\begin{aligned} f_1(x,y) &= a_1 + \sum_{n=1}^{\infty} b_{1n} \cos[n\phi_1(x,y)] \\ f_2(x,y) &= a_2 + \sum_{m=1}^{\infty} b_{2m} \cos[m\phi_2(x,y)] \end{aligned} \tag{16.1}$$

where $\phi(x,y)$ is the function describing the basic shape of the grating lines. For the fundamental frequency, $\phi(x,y)$ is equal to an integer times 2π at the center of each bright line and is equal to an integer plus one-half times 2π at the center of each dark line. The b coefficients determine the profile of the grating lines (i.e., square wave, triangular, sinusoidal, etc). For a sinusoidal line profile, b_{i1} is the only nonzero term.

When these two gratings are superimposed, the resulting intensity transmission function is given by the product

$$\begin{aligned} f_1(x,y)f_2(x,y) = a_1a_2 &+ a_1 \sum_{m=1}^{\infty} b_{2m} \cos[m\phi_2(x,y)] + a_2 \sum_{n=1}^{\infty} b_{1n} \cos[n\phi_1(x,y)] \\ &+ \sum_{m=1}^{\infty} \sum_{n=1}^{\infty} b_{1n}b_{2m} \cos[n\phi_1(x,y)] \cos[m\phi_2(x,y)]. \end{aligned} \tag{16.2}$$

The first three terms of Eq. (16.2) provide information which can be determined by looking at the two patterns separately. The last term is the interesting one, and can be rewritten as

$$\begin{aligned}\text{Term } 4 = &\frac{1}{2} b_{11} b_{21} \cos[\phi_1(x,y) - \phi_2(x,y)] \\ &+ \frac{1}{2} \sum_{m=1}^{\infty} \sum_{n=1}^{\infty} b_{1n} b_{2m} \cos[n\phi_1(x,y) - m\phi_2(x,y)]; n \text{ and } m \text{ both } \neq 1 \\ &+ \frac{1}{2} \sum_{m=1}^{\infty} \sum_{n=1}^{\infty} b_{1n} b_{2m} \cos[n\phi_1(x,y) + m\phi_2(x,y)] \end{aligned} \tag{16.3}$$

This expression shows that by superimposing the two gratings, the sum and difference between the two gratings is obtained. The first term of Eq. (16.3) represents the difference between the fundamental pattern making up the two gratings. It can be used to predict the moiré pattern shown in Figure 16.1. Assuming that two gratings are oriented with an angle 2α between them with the y axis of the coordinate system bisecting this angle, the two grating functions $\phi_1(x,y)$ and $\phi_2(x,y)$ can be written as

$$\phi_1(x,y) = \frac{2\pi}{\lambda_1}(x\cos\alpha + y\sin\alpha)$$

and

$$\phi_2(x,y) = \frac{2\pi}{\lambda_2}(x\cos\alpha - y\sin\alpha) \tag{16.4}$$

where λ_1 and λ_2 are the line spacings of the two gratings. Equation (16.4) can be rewritten as

$$\phi_1(x,y) - \phi_2(x,y) = \frac{2\pi}{\lambda_{\text{beat}}} x\cos\alpha + \frac{4\pi}{\overline{\lambda}} y\sin\alpha \tag{16.5}$$

where $\overline{\lambda} = (\lambda_1 + \lambda_2)/2$ is the average line spacing, and λ_{beat} is the beat wavelength between the two gratings given by

$$\lambda_{\text{beat}} = \frac{\lambda_1 \lambda_2}{\lambda_2 - \lambda_1} \tag{16.6}$$

Note that this beat wavelength is the same that was obtained for two-wavelength interferometry as described in Chapter 15, and is also referred to as the synthetic or equivalent wavelength. Using Eq. (16.3), the moiré or beat will be lines whose centers satisfy the equation

$$\phi_1(x,y) - \phi_2(x,y) = M2\pi \tag{16.7}$$

Three separate cases for moiré fringes can be considered.

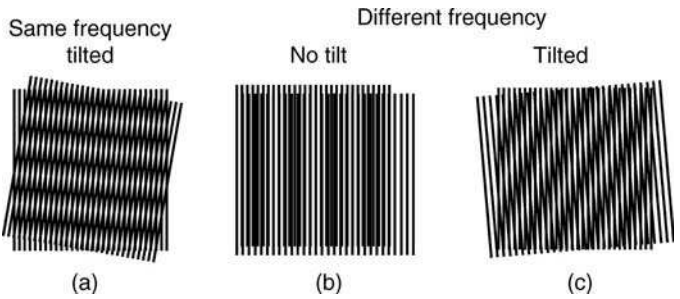

FIGURE 16.2. Moiré patterns caused by two straight line gratings with (a) the same pitch tilted with respect to one another, (b) different frequencies and no tilt, and (c) different frequencies tilted with respect to one another.

For the first case $\lambda_1 = \lambda_2 = \lambda$. The first term of Eq. (16.5) is zero, and the fringe centers are given by

$$M\lambda = 2y \sin \alpha \tag{16.8}$$

where M is an integer corresponding to the fringe order (see Fig. 16.2(a)). As was expected, Eq. (16.8) is the equation of equi-spaced horizontal lines as seen in Fig. 16.1.

For the second simple case $\lambda_1 \neq \lambda_2$ and the gratings are parallel to each other with $\alpha = 0$. This makes the second term of Eq. (16.5) vanish. The moiré will then be lines which satisfy

$$M\lambda_{\text{beat}} = x \tag{16.9}$$

These fringes are equally-spaced lines parallel to the grating lines (see Fig. 16.2(b)).

For the third and more general case where the two gratings have different line spacings $\lambda_1 \neq \lambda_2$ and the angle between the gratings is nonzero $\alpha \neq 0$, the equation for the moiré fringes will now be

$$M\overline{\lambda} = \frac{\overline{\lambda}}{\lambda_{\text{beat}}} x \cos \alpha + 2y \sin \alpha \tag{16.10}$$

This is the equation of straight lines whose spacing and orientation is dependent upon the relative difference between the two grating spacings and the angle between the gratings (see Fig. 16.2(c)).

The orientation and spacing of the moiré fringes for the general case can be determined from the geometry shown in Figure. 16.3 (Chiang, 1983). The distance $\overline{AB}$ can be written in terms of the two grating spacings,

$$\overline{AB} = \frac{\lambda_1}{\sin(\theta - \alpha)} = \frac{\lambda_2}{\sin(\theta + \alpha)} \tag{16.11}$$

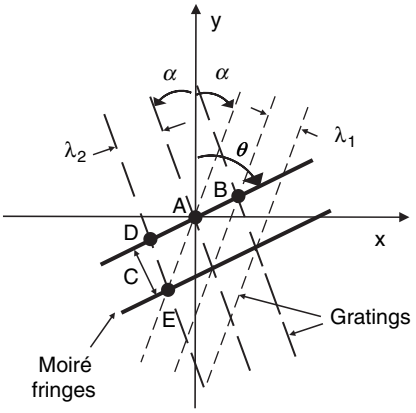

FIGURE 16.3. Geometry used to determine spacing and angle of moiré fringes between two gratings of different frequencies tilted with respect to one another.

where θ is the angle the moiré fringes make with the y axis. After rearranging, the fringe orientation angle θ is given by

$$\tan\theta = \tan\alpha\left(\frac{\lambda_1 + \lambda_2}{\lambda_2 - \lambda_1}\right) \tag{16.12}$$

When $\alpha = 0$ and $\lambda_1 \neq \lambda_2$, $\theta = 0°$, and when $\lambda_1 = \lambda_2$ with $\alpha \neq 0$, $\theta = 90°$ as expected. The fringe spacing perpendicular to the fringe lines can be found by equating quantities for the distance $\overline{DE}$,

$$\overline{DE} = \frac{\lambda_1}{\sin 2\alpha} = \frac{C}{\sin(\theta + \alpha)} \tag{16.13}$$

where C is the fringe spacing or contour interval. This can be rearranged to yield

$$C = \lambda_1\left[\frac{\sin(\theta + \alpha)}{\sin 2\alpha}\right] \tag{16.14}$$

By substituting for the fringe orientation θ, the fringe spacing can be found in terms of the grating spacings and angle between the gratings;

$$C = \frac{\lambda_1\lambda_2}{\sqrt{\lambda_2^2 \sin^2 2\alpha + (\lambda_2 \cos 2\alpha - \lambda_1)^2}} \tag{16.15}$$

In the limit that $\alpha = 0$ and $\lambda_1 \neq \lambda_2$, the fringe spacing equals λ_{beat}, and in the limit that $\lambda_1 = \lambda_2 = \lambda$ and $\alpha \neq 0$, the fringe spacing equals $\lambda/(2\sin\alpha)$. It is possible to determine λ_2 and α from the measured fringe spacing and orientation as long as λ_1 is known (Chiang, 1983).

16.1.3. Moiré and Interferograms

Now that we have covered the basic mathematics of moiré patterns, let us see how moiré patterns are related to interferometry. The single grating shown in Figure 16.1 can be thought of as a "snapshot" of plane waves (like in a collimated beam) traveling to the right where the distance between the grating lines is equal to the wavelength of light. Superimposing the two sets of grating lines in Fig. 16.1b can be thought of as superimposing two plane waves with an angle of 2α between their directions of propagation. When the two waves are in phase, bright fringes result (constructive interference) and when they are out of phase, dark fringes result (destructive interference). For a collimated plane wave, the "grating" lines are really planes (sheets) perpendicular to the plane of the figure and the dark and bright fringes are also planes perpendicular to the plane of the figure. If the plane waves are traveling to the right, these fringes would be observed by placing a screen perpendicular to the plane of the figure and to the right of the grating lines as shown in Figure 16.1. The spacing of the interference fringes on the screen is given by Eq. (16.8), where λ is now the wavelength of light. Thus, the moiré of two straight-line gratings correctly predicts the centers of the interference fringes produced by interfering two plane waves. Since the gratings used to produce the moiré pattern are binary gratings, the moiré does not correctly predict the sinusoidal intensity profile of the interference fringes. (If both gratings had sinusoidal intensity profiles, the resulting moiré would still not have a sinusoidal intensity profile because of higher-order terms.)

More complicated gratings, such as circular gratings, can also be investigated. Figure 16.4(b) shows the superposition of two identical circular grating patterns shown in Figure 16.4(a). This composite pattern indicates the fringe positions obtained by interfering two spherical wavefronts. The centers of the two circular gratings can be considered the source locations for two spherical waves. Just as for two plane waves, the spacing between the grating lines is equal to the wavelength of light. When the two patterns are in phase, bright fringes are produced, and when the patterns are completely out of phase, dark fringes result. For a point on a given fringe, the difference in the distances from the two source points and the fringe point is a constant. Hence, the fringes are hyperboloids. Due to symmetry, the fringes seen on observation plane A of Figure 16.4(b) must be circular. (Plane A is along the top of Fig. 16.4(b) and perpendicular to the line connecting the two sources as well as perpendicular to the page.) Figure 16.4(c) shows a representation of these interference fringes and represents the interference pattern obtained by interfering a non-tilted plane wave and a spherical wave. (A plane wave can be thought of as a spherical wave with an infinite radius of curvature.) Figure 16.4(d) shows that the interference fringes in plane B are essentially straight equi-spaced fringes going into the page. (These fringes are strictly speaking still hyperbolas, but in the limit of large distances, they are essentially straight lines. Plane B is along the side of Fig. 16.4(b) and parallel to the line connecting the two sources as well as perpendicular to the page.)

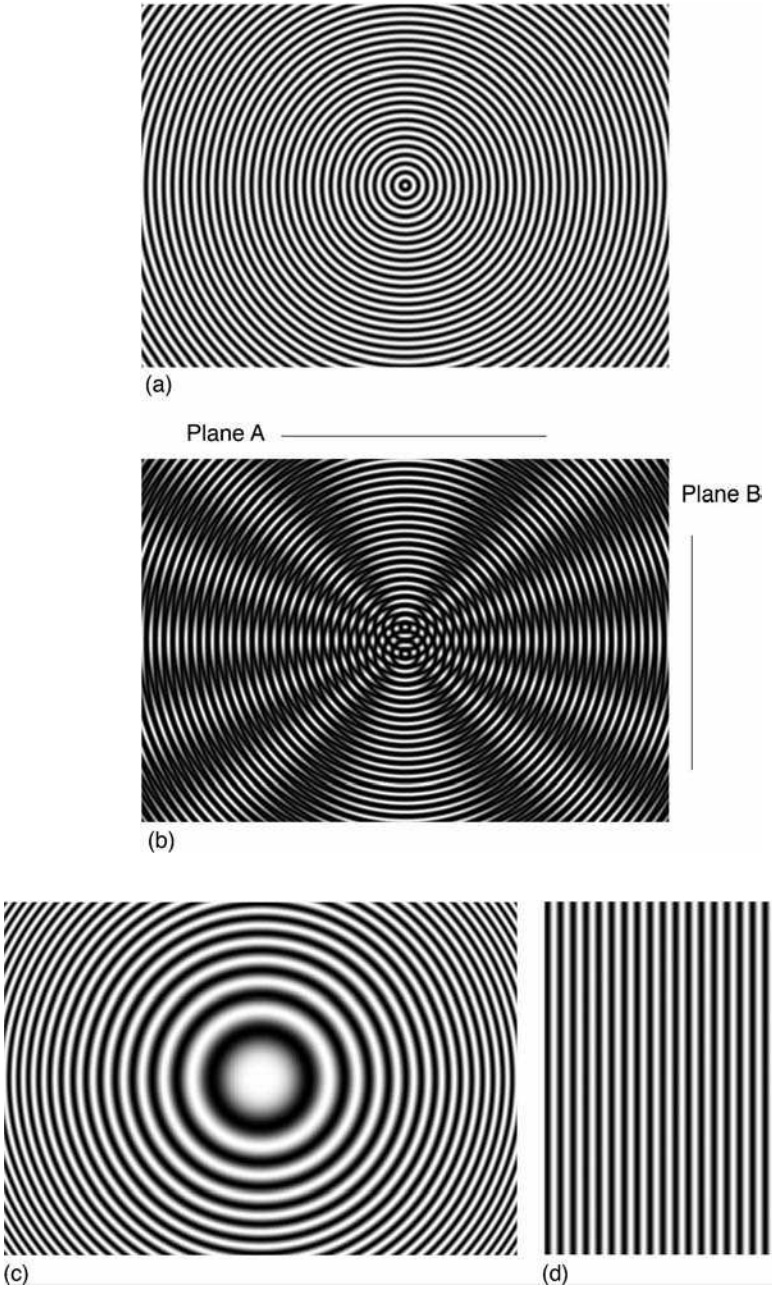

FIGURE 16.4. Interference of two spherical waves. (a) Circular line grating representing a spherical wavefront. (b) Moiré pattern obtained by superimposing two circular line patterns. (c) Fringes observed in plane A. (d) Fringes observed in plane B.

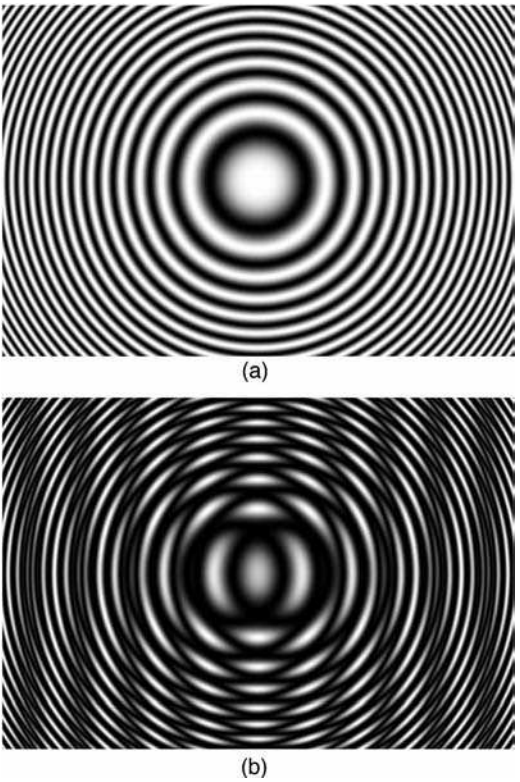

FIGURE 16.5. Moiré pattern produced by two zone plates. (a) Zone plate. (b) Straight line fringes resulting from superposition of two zone plates.

The lines of constant phase in plane B, if there were only a single spherical wave (single point source), are shown in Figure 16.5(a). (To first-order, the lines of constant phase in plane B are the same shape as the interference fringes in plane A.)

The pattern shown in Figure 16.5(a) is commonly called a zone plate. Figure 16.5(b) shows the superposition of two linearly displaced zone plates. The resulting moiré pattern of straight equi-spaced fringes illustrates the interference fringes in plane B shown in Figure 16.4(b).

Superimposing two interferograms and looking at the moiré or beat produced can be extremely useful. The moiré formed by superimposing two different interferograms shows the difference in the aberrations of the two interferograms. For example, Figure 16.6 shows the moiré produced by superimposing two computer-generated interferograms. One interferogram has 20 waves of tilt across the radius (Fig. 16.6(a)), while the second interferogram has 20 waves of tilt plus 4 waves of defocus (Fig. 16.6(b)). If the interferograms are aligned such that the tilt direction is the same for both interferograms, the tilt will cancel and only the 4 waves of defocus remain (Fig. 16.6(c)). In Figure 16.6(d), the two interferograms are rotated slightly

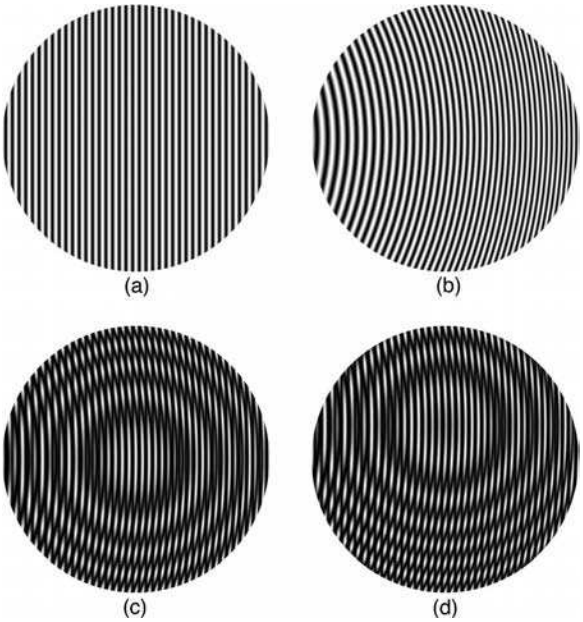

FIGURE 16.6. Moiré between two interferograms. (a) Interferogram having 20 waves tilt. (b) Interferogram having 20 waves tilt plus 4 waves of defocus. (c) Superposition of 16.6a and 16.6b with no tilt between patterns. (d) Slight tilt between patterns.

with respect to each other so that the tilt will not quite cancel. These results can be described mathematically by looking at the two grating functions:

$$\phi_1(x, y) = 2\pi(20\rho\cos\varphi + 4\rho^2)$$

and

$$\phi_2(x, y) = 2\pi[20\rho\cos(\varphi + \alpha)] \tag{16.16}$$

A bright fringe is obtained when

$$\frac{\phi_1 - \phi_2}{2\pi} = 20\rho[\cos\varphi - \cos(\varphi + \alpha)] + 4\rho^2 = M \tag{16.17}$$

If $\alpha = 0$, the tilt cancels completely and 4 waves of defocus remain; otherwise, some tilt remains in the moiré pattern.

Figure 16.7 shows similar results for interferograms containing third-order aberrations. A computer-generated interferogram having 22 waves of tilt across the radius, 4 waves of spherical and -2 waves of defocus is shown in Figure 16.7(a). Net spherical aberration with defocus and tilt is shown in Figure 16.7(d). This is the result of moiré between the interferogram in Figure 16.7(a) with an interferogram

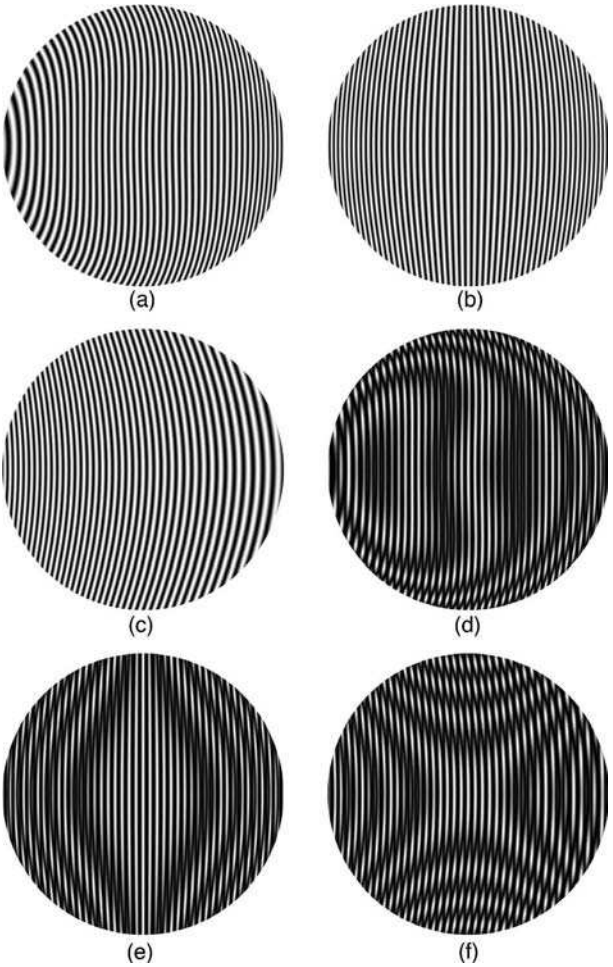

FIGURE 16.7. Moiré patterns showing third-order aberrations. Interferograms containing (a) 22 waves tilt, 4 waves of third-order spherical aberration, and −2 waves of defocus, (b) 20 waves tilt and 5 waves coma, and (c) 20 waves tilt, 7 waves astigmatism, and −3.5 waves of defocus. (d) Moiré pattern between Figure 16.6a and 16.7a. (e) Moiré pattern between Figures 16.6(a) and 16.7(b). (f) Moiré pattern between Figures 16.6(a) and 16.7(c).

having 20 waves of tilt (Fig. 16.6(a)). Figure 16.7(e) shows the moiré between an interferogram having 20 waves of tilt (Fig. 16.6(a)) with an interferogram having 20 waves of tilt and 5 waves of coma (Fig. 16.7(b)) netting 5 waves of coma in the moiré. The moiré between an interferogram having 20 waves of tilt (Fig. 16.6(a)) and one having 20 waves of tilt, 7 waves third-order astigmatism, and −3.5 waves defocus (Fig. 16.7(c)) is shown in Figure 16.7(f). Thus, it is possible to produce simple fringe patterns using moiré. These patterns can be printed or photocopied onto transparencies and used as a learning aid to understand interferograms obtained from

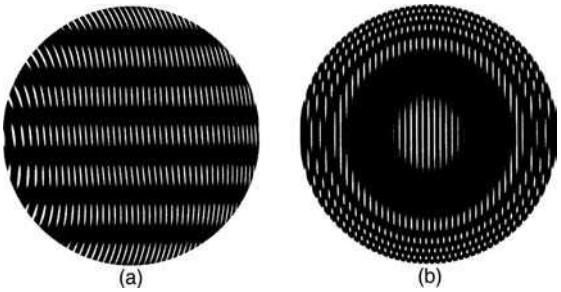

FIGURE 16.8. Moiré pattern by superimposing two identical interferograms (Figure 16.7(a)). (a) Both patterns having the same orientation. (b) One pattern is flipped.

third-order aberrations. Electronic copies are available at JC Wyant's website (Wyant, 2006) as well as on the accompanying CD to this book.

Figure 16.8(a) shows two identical interferograms superimposed with a small rotation between them. As we might by now expect, the moiré pattern consists of nearly straight equi-spaced lines. However, when one of the two interferograms is flipped over, the aberrations will add rather than subtract, and the resultant moiré is shown in Figure 16.8(b). When one interferogram is flipped, the fringe deviation from straightness in one interferogram is to the right and, in the other, to the left. Thus, the signs of the defocus and spherical aberration for the two interferograms are opposite and the resulting moiré pattern has twice the defocus and spherical of each of the individual interferograms.

When two identical interferograms given by Figure 16.7(a) are superimposed with a displacement from one another, a shearing interferogram is obtained. Figure 16.9 shows vertical and horizontal displacements with and without a rotation between the two interferograms. The rotations indicate the addition of tilt to the interferograms. These types of moiré patterns are very useful for understanding lateral shearing interferograms.

Moiré patterns are produced by multiplying two intensity distribution functions. Adding two intensity functions does not give the difference term obtained in Eq. (16.3). A moiré pattern is not obtained if two intensity functions are added. The only way to get a moiré pattern by adding two intensity functions is to use a nonlinear detector. For the detection of an intensity distribution given by $I_1 + I_2$, a nonlinear response can be written as

$$\text{Response} = a(I_1 + I_2) + b(I_1 + I_2)^2 + \cdots \tag{16.18}$$

This produces terms proportional to the product of the two intensity distributions in the output signal. Hence, a moiré pattern is obtained if the two individual intensity patterns are simultaneously observed by a nonlinear detector (even if they are not multiplied before detection). If the detector produces an output linearly proportional to the incoming intensity distribution, the two intensity patterns must be multiplied to produce the moiré pattern. Since the eye is a nonlinear detector, moiré can be seen

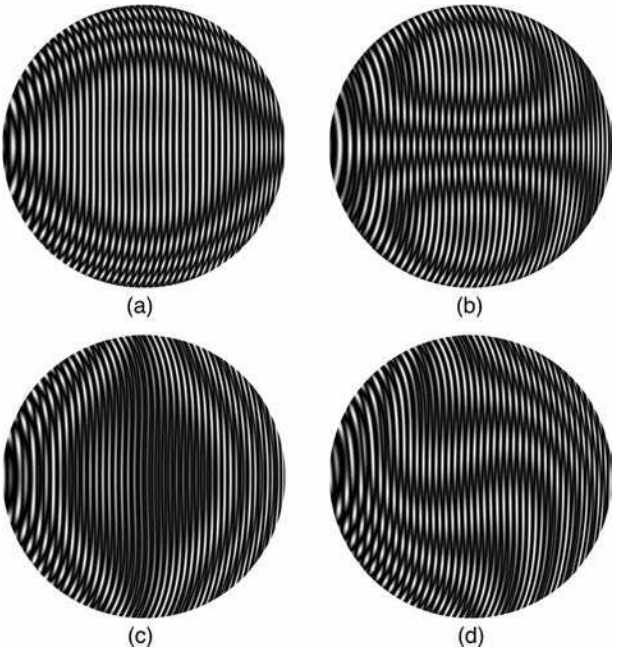

FIGURE 16.9. Moiré patterns formed using two identical interferograms (Figure 16.7(a)) where the two are sheared with respect to one another. (a) Vertical displacement. (b) Vertical displacement with rotation showing tilt. (c) Horizontal displacement. (d) Horizontal displacement with rotation showing tilt.

whether the patterns are added or multiplied. A good TV camera, on the other hand, will not see moiré unless the patterns are multiplied.

16.1.4. Historical Review

Since Lord Rayleigh first noticed the phenomena of moiré fringes, moiré techniques have been used for a number of testing applications. Righi (1887) first noticed that the relative displacement of two gratings could be determined by observing the movement of the moiré fringes. The next significant advance in the use of moiré was presented by Weller and Shepherd (1948). They used moiré to measure the deformation of an object under applied stress by looking at the differences in a grating pattern before and after the applied stress. They were the first to use shadow moiré, where a grating is placed in front of a nonflat surface, to determine the shape of the object behind it by using the shape of the moiré fringes. A rigorous theory of moiré fringes did not exist until the mid-fifties when Ligtenberg (1955) and Guild (1956, 1960) explained moiré for stress analysis by mapping slope contours and displacement measurement, respectively. Excellent historical reviews of the early work in moiré have been presented by Theocaris (1962, 1966). Books on this subject have been written by Guild (1956, 1960), Theocaris (1969), and Durelli and Parks (1970). Projection moiré techniques were introduced by Brooks and Helfinger (1969) for

optical gauging and deformation measurement. Until 1970, advances in moiré techniques occurred mostly in stress analysis. Some of the first uses of moiré to measure surface topography were reported by Meadows et al., (1970), Takasaki (1970), and Wasowski (1970). Moiré has also been used to compare an object to a master and for vibration analysis (Der Hovanesian and Yung, 1971; Gasvik, 2002). A theoretical review and experimental comparison of moiré and projection techniques for contouring is given by Benoit et al. (1975). Automatic computer fringe analysis of moiré patterns by finding fringe centers was reported by Yatagai et al. (1982). Heterodyne interferometry was first used with moiré fringes by Moore and Truax (1979), and phase measurement techniques were further developed by Perrin and Thomas (1979), Shagam (1980), and Reid (1984b). Review papers on moiré techniques include Post (1982), Reid (1984a), and Halioua and Liu (1989) and recent books include Patorski and Kujawinska (1993), Post et al. (1997), Amridror (2000), and Walker (2004).

The projection of interference fringes for contouring objects was first proposed by Rowe and Welford (1967). Their later work included a number of applications for projected fringes (Welford, 1969) and the use of projected fringes with holography (Rowe, 1971). In-depth mathematical treatments have been provided by Benoit et al. (1975) and Gasvik (2002). The relationship between projected fringe contouring and triangulation is given in a book chapter by Case et al. (1987). Heterodyne phase measurement was first introduced with projected fringes by Indebetouw (1978), and phase measurement techniques were further developed by Takeda, Ina, and Kabayashi (1982), Takeda and Mutoh (1983), and Srinivasan, Liu, and Halioua (1984, 1985). Today phase measurement techniques are the norm as described in the list of recent books listed above.

Haines and Hildebrand first proposed contouring objects in holography using two sources (Haines and Hildebrand, 1965; Hildebrand and Haines, 1966, 1967). These two sources were produced by changing either the angle of the illumination beam on the object or the angle of the reference beam. A small angle difference between the beams used to produce a double-exposure hologram creates a moiré in the final hologram which corresponded to topographic contours of the test object. Further insight into two-angle holography has been provided by Menzel (1974), Abramson (1976a,b), and DeMattia and Fossati-Bellani (1978). The technique has also been used in speckle interferometry (Winther, 1983). These holographic and speckle techniques are described more in the second half of this chapter.

Since all of these techniques are so similar, it is sometimes hard to differentiate developments in one technique versus another. MacGovern (1972) provided a theory that linked all of these techniques together. The next part of this chapter will explain each of these techniques and then show the similarities among all of these techniques and provide a comparison to conventional interferometry.

16.1.5. Fringe Projection

A simple approach for contouring is to project interference fringes or a grating onto an object and then view from another direction. Figure 16.10 shows the optical

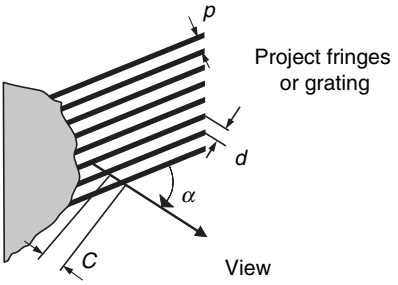

FIGURE 16.10. Projection of fringes or grating onto object and viewed at an angle α. p is the grating pitch or fringe spacing and C is the contour interval.

setup for this measurement. Assuming a collimated illumination beam and viewing the fringes with a telecentric optical system, straight equally-spaced fringes are incident on the object producing equally-spaced contour intervals. The departure of a viewed fringe from a straight line shows the departure of the surface from a plane reference surface. An object with fringes of spacing p projected onto it can be seen in Figure 16.11. When the fringes are viewed at an angle α relative to the projection direction, the spacing of the lines perpendicular to the viewing direction will be

$$d = \frac{p}{\cos \alpha} \tag{16.19}$$

The contour interval C (the height between adjacent contour lines in the viewing direction) is determined by the line or fringe spacing projected onto the surface and the angle between the projection and viewing directions;

$$C = \frac{p}{\sin \alpha} = \frac{d}{\tan \alpha} \tag{16.20}$$

These contour lines are planes of equal height and the sensitivity of the measurement is determined by α. The larger the angle α, the smaller the contour interval. If $\alpha = 90^\circ$, then the contour interval is equal to p, and the sensitivity is a maximum. The reference plane will be parallel to the direction of the fringes and perpendicular to the viewing direction as shown in Figure 16.12. Even though the maximum sensitivity can be obtained, a 90° angle between the projection and viewing directions will produce a lot of unacceptable shadows on the object. These shadows will lead to areas with missing data where the object cannot be contoured. When $\alpha = 0$, the contour interval is infinite, and the measurement sensitivity is zero. To provide the best results, an angle no larger than the largest slope on the surface should be chosen.

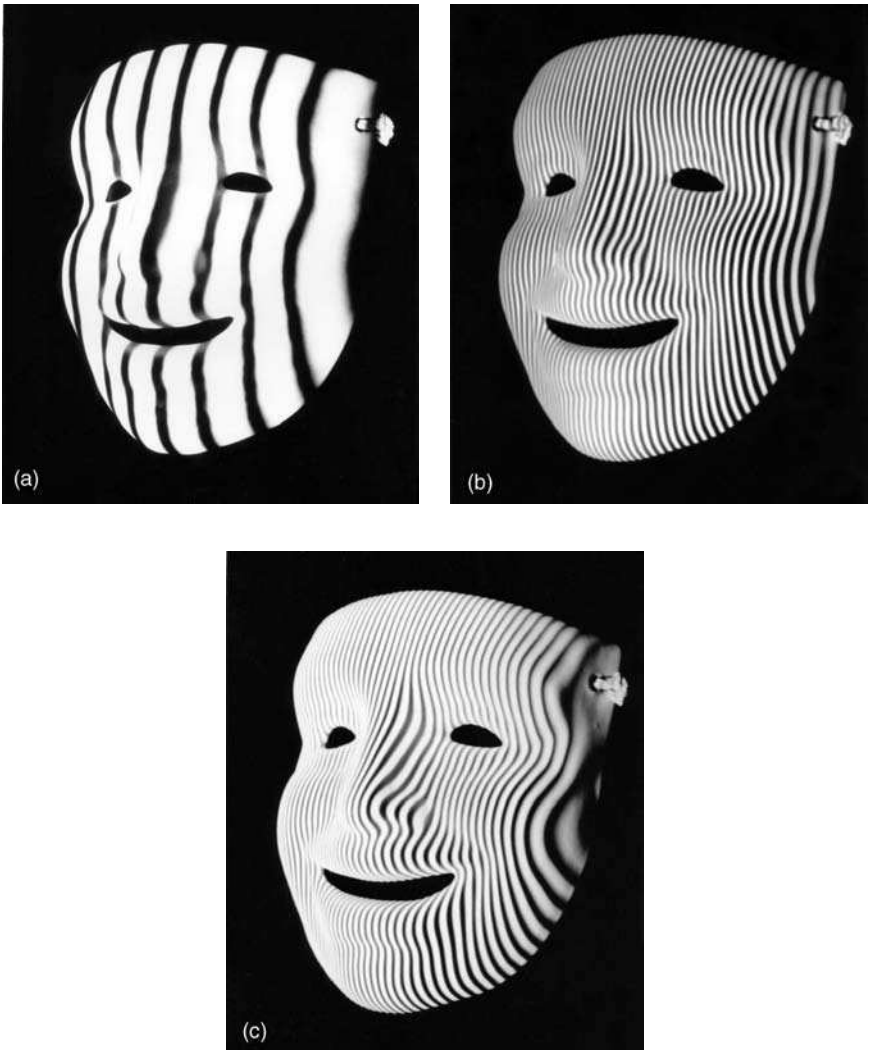

FIGURE 16.11. Mask with fringes projected onto it. (a) Coarse fringe spacing. (b) Fine fringe spacing. (c) Fine fringe spacing with an increase in the angle between illumination and viewing.

When interference fringes are projected onto a surface rather than using a grating, the fringe spacing p is determined by the geometry shown in Figure 16.13 and is given by

$$p = \frac{\lambda}{2 \sin \Delta\theta} \tag{16.21}$$

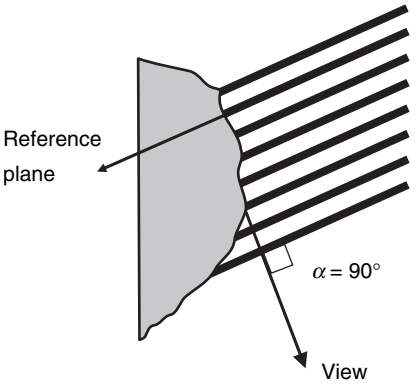

FIGURE 16.12. Maximum sensitivity for fringe projection with a 90° angle between projection and viewing.

where λ is the wavelength of illumination and $2\Delta\theta$ is the angle between the two interfering beams. Substituting the expression for p into Eq. (16.20), the contour interval becomes

$$C = \frac{\lambda}{2(\sin\Delta\theta)\sin\alpha} \tag{16.22}$$

If a simple interferometer such as a Twyman–Green is used to generate projected interference fringes, tilting one beam with respect to the other will change the contour interval. The larger the angle between the two beams, the smaller the contour interval will be. Figures 16.11(a and b) show a change in the fringe spacing for interference fringes projected onto an object. The direction of illumination has been moved away from the viewing direction between Figures 16.11(b and c). This increases the angle α and the test sensitivity while reducing the contour interval. Projected fringe contouring has been covered in detail by Gasvik (2002).

If the source and the viewer are not at infinity, the fringes or grating projected onto the object will not be composed of straight, equally-spaced lines. The height between contour planes will be a function of the distance from the source and viewer to the object. There will be a distortion due to the viewing of the fringes as well as due to the illumination. This means that the reference surface will not be a plane. As long as the object does not have large height changes compared to the illumination and viewing distances, a plane reference surface placed in the plane of the object can be

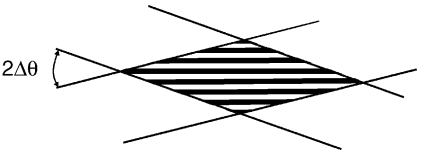

FIGURE 16.13. Fringes produced by two interfering beams.

measured first and then subtracted from subsequent measurements of the object. This enables the mapping of a plane in object space to a surface which will serve as a reference surface. If the object has large height variations, the plane reference surface may have to be measured in a number of planes to map the measured object contours to real heights. Finite illumination and viewing distances will be considered in more detail with shadow moiré in Section 16.1.6.

Fringe Projection using Microdisplays. For many years fringe projection methods relied on Ronchi gratings, which were often made as imprinted chrome lines on a glass substrate, but present-day systems employ a number of different types of microdisplays (digital light projectors); three commonly-used types of microdisplays (Armitage et al., 2002), namely micro-electro-mechanical-systems (MEMS), liquid-crystal and electroluminescent technologies, allow for active addressing of individual pixels high resolution matrix display area. The first type, which includes digital micromirror displays (DMD – Texas Instrument trademark), uses an array of individual, approximately 13 μm square mirrors that are switched on and off at different frequencies so as to obtain different levels of projected light. The second type of microdisplays are liquid crystal displays (LCD), where standard LCDs are build of twisted nematic liquid crystal layers and work in transmission. The newer type of LCDs is based on ferroelectric crystal placed on silicon (LCoS) and works in reflection. LCD displays act as spatial light modulators (SLM) and require incident polarized light. The third type is microdisplay made of an array of organic (polymer) light emitting diodes (OLEDS or PLEDS). This type is best suited for small systems because pixels made of organic polymers are Lambertian emitters itself and do not require additional illuminator. The advantage of any fringe projection system using microdisplays controlled by computer is that they do not require a mechanical phase shifting grating and the type of projected fringes can be changed with a mouse click. Fringes are changed by addressing pixels of microdisplay. Additional advantage of microdisplays is that the period and brightness (Kowarschik et al., 2000; Proll et al., 2003) of light patterns can be adapted to the type of object and also patterns can be displayed in different colors allowing for simultaneous collection of three patterns with color CCD camera. Many authors have analyzed performance of microdisplays in fringe projection for shape measurement (Frankowski et al., 2000; Proll et al., 2003; Notni, Riehemann et al., 2004).

16.1.6. Shadow Moiré

A simple method of moiré interferometry for contouring objects uses a single grating placed in front of the object as shown in Figure 16.14. The grating in front of the object produces a shadow on the object which is viewed from a different direction through the grating. A low frequency beat or moiré pattern is seen. This pattern is due to the interference between the grating shadows on the object and the grating as viewed. Assuming that the illumination is collimated and that the object is viewed at infinity or through a telecentric optical system, the height z between the grating and

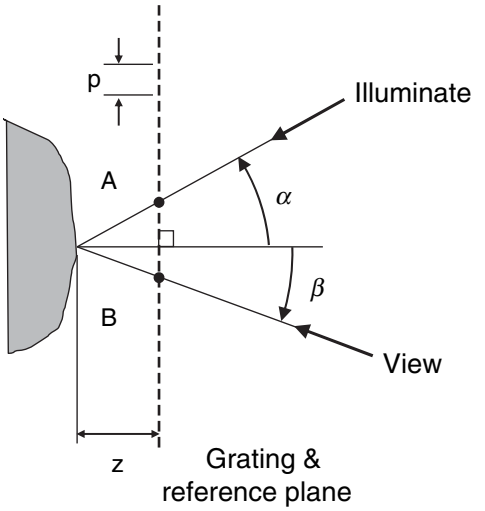

FIGURE 16.14. Geometry for shadow moiré with illumination and viewing at infinity, that is, parallel illumination and viewing.

the object point can be determined from the geometry shown in Figure 16.14 (Meadows et al., 1970; Takasaki, 1973; Chiang, 1983). This height is given by

$$z = \frac{Np}{\tan\alpha + \tan\beta} \tag{16.23}$$

where α is the illumination angle, β is the viewing angle, p is the spacing of the grating lines, and N is the number of grating lines between the points A and B (see Fig. 16.14). The contour interval in a direction perpendicular to the grating will simply be given by

$$C = \frac{p}{\tan\alpha + \tan\beta} \tag{16.24}$$

Again, the distance between the moiré fringes in the beat pattern depends upon the angle between the illumination and viewing directions. The larger the angle, the smaller the contour interval. If the high frequencies due to the original grating are filtered out, then only the moiré interference term is seen. The reference plane will be parallel to the grating. Note that this reference plane is tilted with respect to the reference plane obtained when fringes are projected onto the object. Essentially, the shadow moiré technique provides a way of removing the ''tilt'' term and repositioning the reference plane. The contour interval for shadow moiré is the same as that calculated for projected fringe contouring [Eq. (16.20)] when one of the angles is zero with $d = p$. Figure 16.15 shows an object which has a grating sitting in front of it. An illumination beam is projected from one direction and viewed

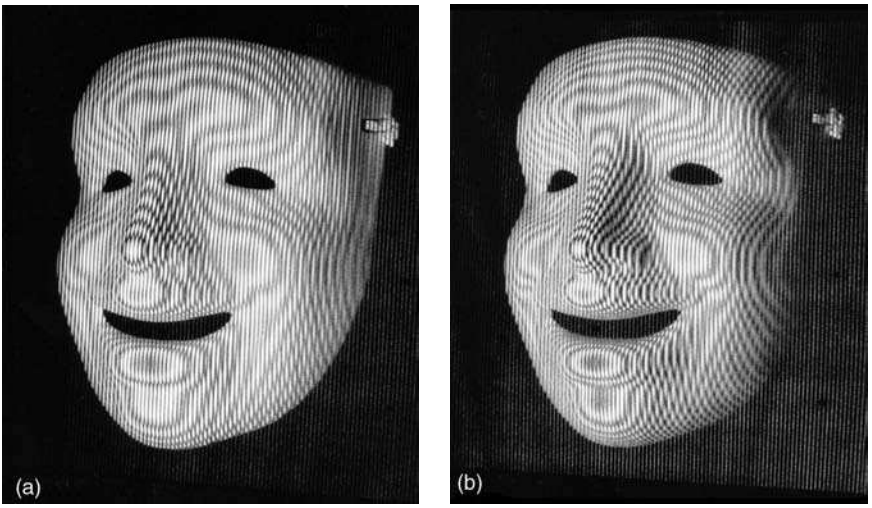

FIGURE 16.15. Mask with grating in front of it. (a) One viewing angle. (b) Larger viewing angle.

from another direction. Between Figures 16.15a and b, the angles α and β have been increased. This has the effect of decreasing the contour interval, increasing the number of fringes, and rotating the reference plane slightly away from the viewer.

Most of the time, it is difficult to illuminate an entire object with a collimated beam. Therefore, it is important to consider the case of finite illumination and viewing distances. It is possible to derive this for a very general case (Meadows, Johnson, and Allen, 1970; Takasaki, 1970; Bell, 1985); however, for simplicity, only the case where the illumination and viewing positions are the same distance from the grating will be considered. Figure 16.16 shows a geometry where the distance between the illumination source and the viewing camera is given by w, and the distance between these and the grating is l. The grating is assumed to be close enough to the object surface so that diffraction effects are negligible. In this case, the height between the object and the grating is given by

$$z = \frac{Np}{\tan\alpha' + \tan\beta'} \tag{16.25}$$

where α' and β' are the illumination and viewing angles at the object surface. These angles change for every point on the surface and are different from α and β in Figure 16.16 which are the illumination and viewing angles at the grating (reference) surface. The surface height can also be written as (Meadows et al., 1970; Takasaki, 1973; Chiang, 1983)

$$z = NC(z) = \frac{Np(l+z)}{w} = \frac{Npl}{w - Np} \tag{16.26}$$

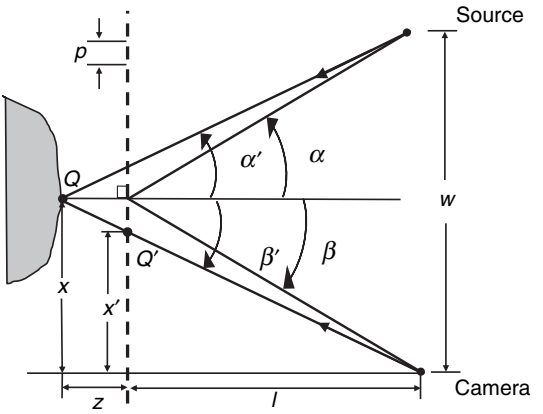

FIGURE 16.16. Geometry for shadow moiré with illumination and viewing at finite distances.

This equation indicates that the height is a complex function depending upon the position of each object point. Thus, the distance between contour intervals is dependent upon the height on the surface and the number of fringes between the grating and the object. Individual contour lines will no longer be planes of equal height. There are now surfaces of equal height. The expression for height can be simplified by considering the case where the distance to the source and viewer is large compared to the surface height variations, $l \gg z$. Then the surface height can be expressed as

$$z = \frac{Npl}{w} = \frac{Np}{\tan\alpha + \tan\beta} \tag{16.27}$$

Even though the angles α and β vary from point-to-point on the surface, the sum of their tangents remains equal to w/l for all object points as long as $l \gg z$. The contour interval will be constant in this regime and will be the same as that given by Eq. (16.24).

Because of the finite distances, there is also distortion due to the viewing perspective. A point on the surface Q will appear to be at the location Q' when viewed through the grating. By similar triangles, the distances x and x' from a line perpendicular to the grating intersecting the camera location can be related using

$$\frac{x}{z+l} = \frac{x'}{l} \tag{16.28}$$

where x and x' are defined in Figure 16.16. Equation (16.28) can be rearranged to yield the actual coordinate x in terms of the measured coordinate x' and the

measurement geometry,

$$x = x'\left(1 + \frac{z}{l}\right) \tag{16.29}$$

Likewise, the y coordinate can be corrected using

$$y = y'\left(1 + \frac{z}{l}\right) \tag{16.30}$$

This enables the measured surface to be mapped to the actual surface to correct for the viewing perspective. These same correction factors can be applied to fringe projection.

16.1.7. Projection Moiré

Moiré interferometry can also be implemented by projecting interference fringes or a grating onto an object and then viewing through a second grating in front of the viewer (see Fig. 16.17) (Brooks and Helfinger, 1969). Instead of using a second grating to observe moiré fringes, the spacing of pixels on a digital camera can be used if the pitch is close to the observed fringe spacing (Bell 1985).

The difference between projection and shadow moiré is that in projection moiré two different gratings are used in projection moiré. The orientation of the reference plane can be arbitrarily changed by using different grating pitches to view the object. The contour interval is again given by Eq. (16.24), by substituting a period of $d = p/\cos a$ for p where a is the angle of illumination direction. Fringes of spacing p or a grating of pitch p perpendicular to the direction of illumination will have a period of $d = p/\cos a$ in the y plane (see Fig. 16.16). As long as the grating pitches are matched for both illumination and viewing to have the same value of d in the y plane then the contour interval can be found using Eq. (16.24) with d substituted for p. This implementation makes projection moiré the same as shadow moiré, although

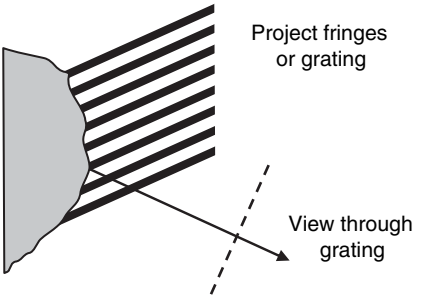

FIGURE 16.17. Projection moiré where fringes or a grating are projected onto a surface and viewed through a second grating.